CB Report 337

$\bar{p}p \to \pi^0\pi^0$ in flight

D.V. Bugg and A. Sarantsev

1 Abstract

Differential cross sections for $\bar{p}p \to \pi^0\pi^0$ at momenta from 600 to 1940 MeV/c are presented, and fitted to partial waves. The amplitude analysis finds two alternative solutions, one of which agrees with earlier analyses of $\bar{p}p \to \pi^-\pi^+$, while the other does not. Both solutions require contributions from $f_4(2050)$ and $f_4(2300)$; the latter has mass $M = 2295 \pm 15$ MeV in the two solutions and width 230 ± 25 MeV, close to earlier determinations. Both solutions also require an f_2 with $M = 2010 \pm 25$ MeV, $\Gamma = 180 \pm 35$ MeV. These f_2 and f_4 resonances agree closely with Bing Song Zou's analysis of $\bar{p}p \to \eta\pi^0\pi^0$ in flight. We interpret the $f_2(2010)$ as the $^3F_2$ $\bar{q}q$ state expected close to $f_4(2050)$.

2 Processing of Data

This follows standard procedures for reconstruction and kinematic fitting agreed with Bochum early in 1997. Packages used for reconstruction are:

– CBar General Offline Software Version 1.30/09

– Crystal Data Reconstruction Version 2.04/03

– CBKFIT Version 3.09/00

– Brain Version 3.03a

– Fast Fuzzy Pattern Recognition

LOCATOR is not used, since charged particles are not reconstructed, only vetoed. Events with a PED centred in Crystal 13 have NOT been rejected, as has been the practice at rest; it rejects too many events. We rely on overall

energy-momentum balance to reject events where photon energy is lost down the beam-pipe.

For both data and Monte Carlo, all photon energies have been scaled (by $\sim 3\%$), so that the total energy peak in both is centred within 1 MeV at the nominal total energy. We have made tests without this scaling factor and find that less than 1 percent of events are affected; roughly the same number move out of the fit as move in when this change is made. If the energy dependence of the crystal calibration were a problem, the $\pi^0\pi^0$ differential cross section at high beam momenta and small scattering angles should be sensitive to it; it fact we find that the angular distribution is unaffected if the scaling factor is omitted, so we are confident this is not a problem.

Extensive studies were made in April-June 1997 of merged pions and split-offs. Our conclusion, averaged over all categories of events from 4 to 8γ, was that they increase the statistics of accepted events by only 10%, but increase backgrounds substantially (by a factor 10). We therefore decided to drop all merged pions and split-offs. As regards the $\pi^0\pi^0$ channel, this may be a bit severe. Backgrounds are actually very low (well below 1%), so including merged pions and split-offs actually increases background levels only to the level of 1-2%. The effects were much worse for 6γ events and also for $\eta\eta'$. It was convenient to process all types of events in the same way. Consequently, $\pi^0\pi^0$ events have been derived purely from events containing exactly 4 PED's. We reject all events which fit other two-body channels with confidence level greater than $\pi^0\pi^0$. Numbers of accepted events and reconstruction efficiencies are shown in Table 1.

Our general procedure in estimating backgrounds is to generate 20,000 Monte Carlo events for every one of the 43 physics channels we fit kinematically. These Monte Carlo events are then fitted to every channel. From the number fitting the correct channel, we evaluate reconstruction efficiencies. From the number of Monte Carlo events fitting the wrong channels, we estimate probabilities of cross-talk. Using the number of data events fitting every channel, we solve a set of 43 $\times$43 simultaneous equations to determine the branching ratios for every channel and the levels of background due to cross-talk. Algebra is given explicitly in Zou's technical report on $\eta\pi^0\pi^0$ data. In general, we carry out this study of background for a series of different confidence levels (e.g. 1, 5, 10 and 20 %) and for a large number (typically 25) of 'rules' by which events are selected and backgrounds are suppressed. The choice of the best 'rule' is a compromise between high statistics and low backgrounds. However, for $\pi^0\pi^0$, it is not necessary to study many alternatives, since backgrounds are very low. The only backgrounds which are measurable are (a) from $3\pi^0$ after losing two photons ($\sim 0.2\%$ at all momenta) and (b) from $\omega\pi^0$, $\omega \to \pi^0\gamma$ after losing one photon ($\sim 0.1\%$).

Momentum (Mev/c)	Data	Monte Carlo	ϵ (%)
600	36,139	129,225	49.7
900	230,528	143,541	47.8
1050	208,312	129,211	46.1
1200	190,207	166,011	43.7
1350	151,598	145,168	41.4
1525	81,061	114,460	38.2
1642	76,545	105,895	35.3
1800	64,468	76,997	32.1
1940	60,529	77,698	28.8

Table 1
Numbers of data events, number of reconstructed Monte Carlo events and the reconstruction efficiency ϵ v. beam momentum

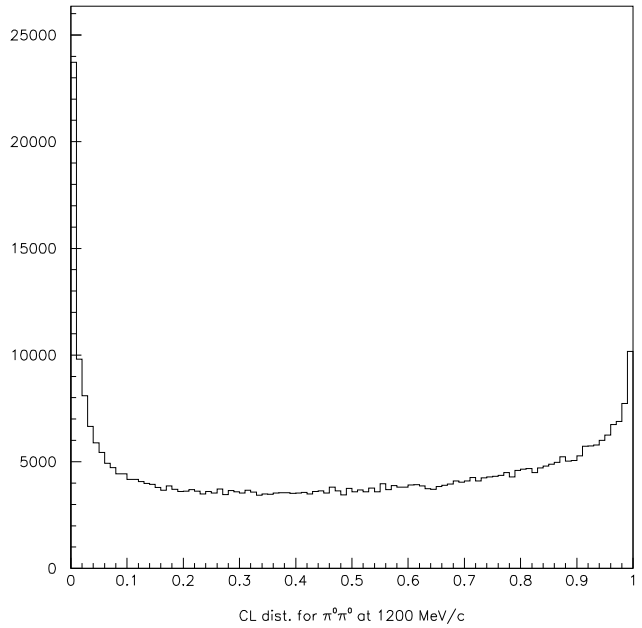

Fig. 1. Confidence level distribution for $\pi^0\pi^0$ events at 1200 MeV/c

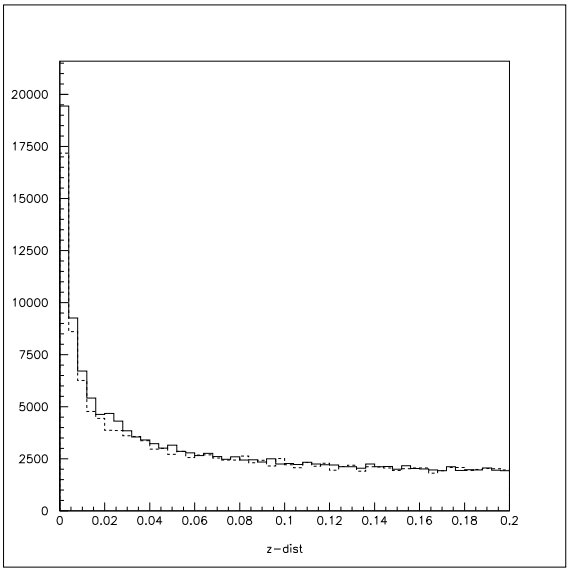

Fig. 2. Blown-up view of the confidence level distribution at 1200 MeV/c for confidence levels below 0.2.

2.1 Confidence Level Distributions

The resulting confidence level distribution is shown in Fig. 1 for a typical case, 1200 MeV/c. There are peaks at both low and high confidence level. The one at high confidence level is due to events with abnormally low errors. These are mostly events at small scattering angles, having one photon close to the beam. These have a larger error on the reconstructed z-coordinate of the vertex, because of the small angles. We apply no cut on the vertex, so that the angular distribution is not biased by different cuts at different scattering angles. The peak at large confidence levels is reproduced well by the Monte Carlo. These events will inevitably be accepted anyway.

Most of the peak at small confidence level is NOT due to backgrounds, but is reproduced by the Monte Carlo down to a confidence level of 1%, as shown in Fig. 2. We have not been able to account fully for the origin of this peak. Some of it certainly arises from events with closely overlapping PEDs, where the separation of the PEDs is ambiguous. To be on the safe side, we have used a conservative confidence level cut of 10%, just where the rise starts. However, we have found that angular distributions obtained with different confidence levels from 1 to 20% agree within statistics. An illustration of this is shown in Fig. 3, where data at 1800 MeV/c are shown for confidence levels of 20% (full line) and 1% (dashed).

In passing, we mention one observation. In the past, some people have applied

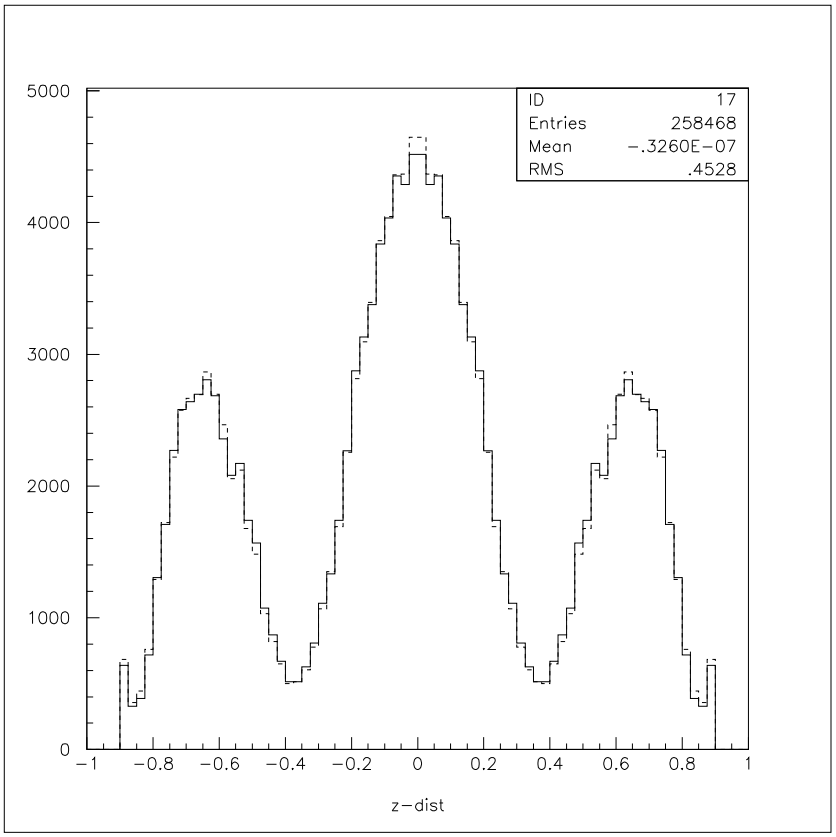

Fig. 3. Comparison of the differential cross section at 1800 MeV/c using confidence level cuts of 20% (full line) and 1% (dashed).

a confidence level cut on fits to 4γ and perhaps $\pi^0\gamma\gamma$. Then they have gone on to apply a further confidence level cut of 10% on $\pi^0\pi^0$. This is NOT a good idea unless the confidence level of the last cut is MUCH higher than at the earlier steps. There are four constraints on the first of these, 5 on the second and 6 on the third. Events may pass one confidence level but not another. The three cuts are correlated. There is a danger of distorting the confidence level distribution severely at the end of the procedure.

2.2 Bad Crystals

A point where care is required is in the treatment of bad crystals. The COLA records were inspected to locate the few occasions when there were missing or inefficient crystals. Likewise, two-dimensional distributions of θ and ϕ were made for PEDS from data. Badly behaved crystals need to be rejected completely, both for data and Monte Carlo. If one does not do this, one bad crystal

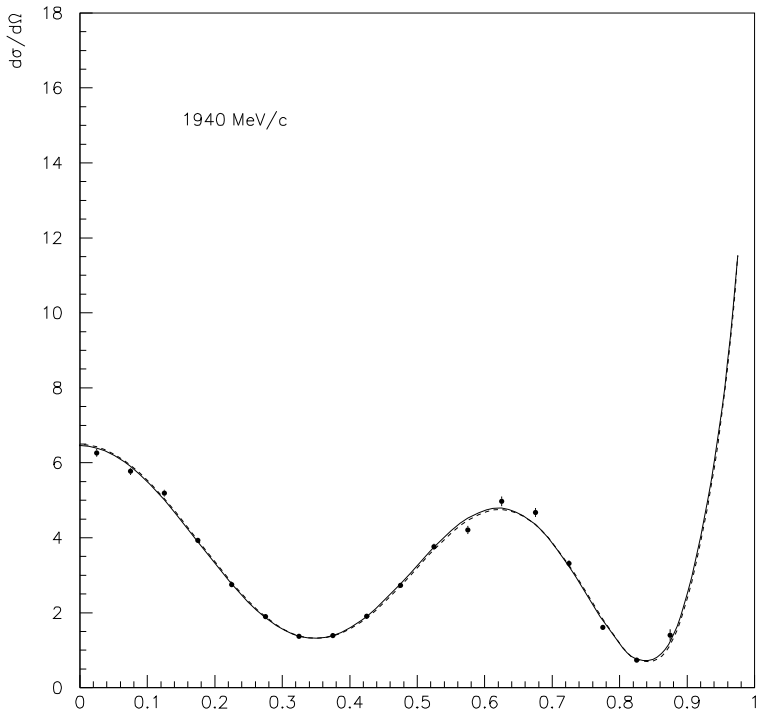

Fig. 4. The angular distribution (in $\mu b/sr$) v. $\cos\theta$, at 1940 MeV/c, compared with solution 1 (full line) and solution 2 (dashed line). These solutions are described below. Here θ is the centre of mass scattering angle.

reduces $d\sigma/d\Omega$ locally in $\cos\theta$. Because of this problem, we decided to reject the WHOLE of the earliest data set at 1200 MeV/c; it amounted to only 25% of the data, and it seemed safest to accept a small statistical loss. The statistics are very high at this momentum anyway.

3 Normalisation

We refer you to the technical report on the in-flight normalisation, technical report 335 and the subsequent addendum, report 336. There, the normalisation of all events fitting as 4 to 8γ was determined. Then we have multiplied by the fraction of these events which fit as $\pi^0\pi^0$. The procedures for evaluating the cross section integrated for $\cos\theta = 0$ to 0.85 are explained there.

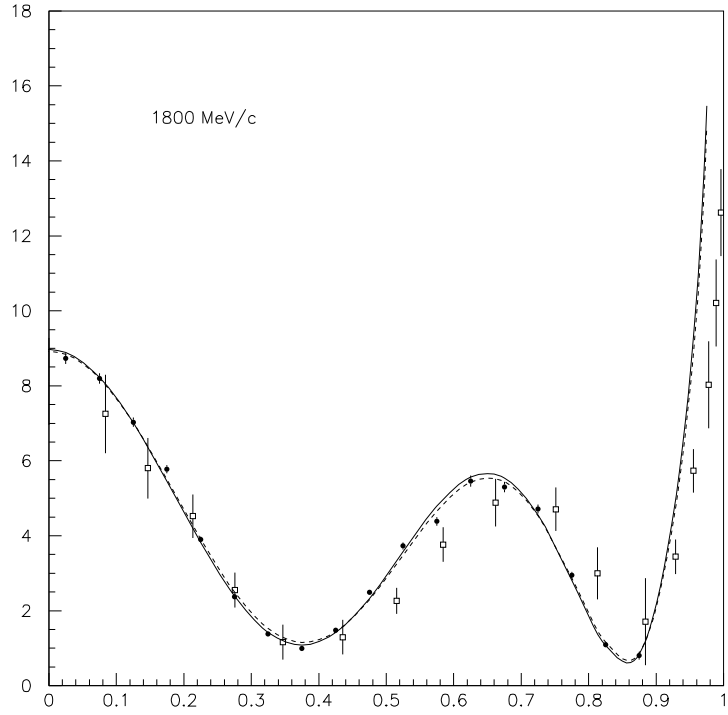

Fig. 5. As Fig. 4 at 1800 MeV/c. Open circles show results of Dulude et al. at 1799 MeV/c after renormalising them to give the best agreement with Crystal Barrel data.

4 Results

Angular distributions are shown in Figs. 4 to 6 at momenta from 1940 to 1642 MeV/c. Statistical errors of Monte Carlo acceptance and data have been compounded. A 0.3% background is assumed to be isotropic and has been subtracted. The dotted curves show the acceptance. It drops sharply at about $\cos\theta = 0.85$. We discard all events above $\cos\theta = 0.9$ and double the statistical errors for $\cos\theta = 0.85$ to 0.9.

The acceptance shows an irregular structure v. $\cos\theta$, particularly at high momenta. It is independent of any cuts applied to the data. It originates from the finite size of the crystals. Fig. 7 shows a plot of individual PEDs from data in bins of $\cos\theta$. There is a conspicuous regular pattern. The software is unable to generate accurately the locations of PEDS within a crystal and the distributions peak at the centres of crystals. Despite the random angles of

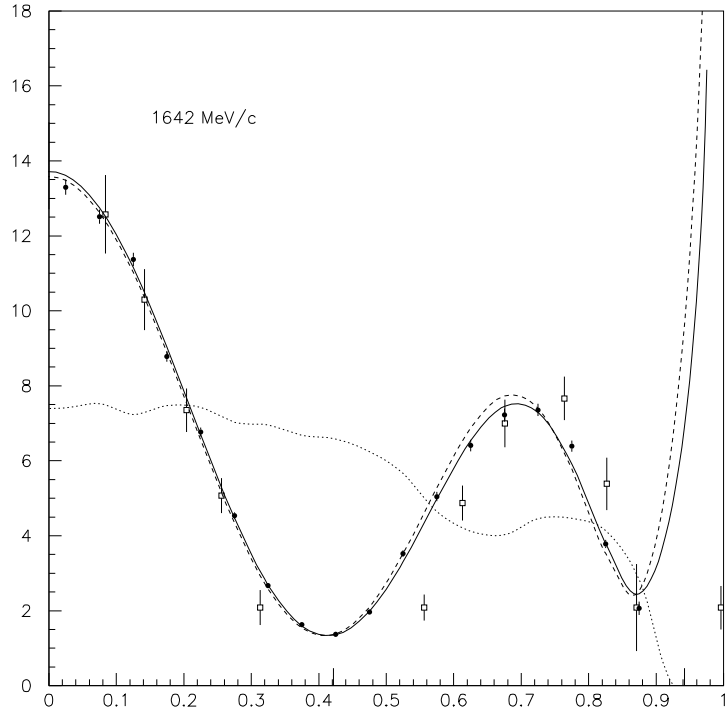

Fig. 6. As Fig. 4 at 1800 MeV/c. The dotted curve shows the acceptance derived from the Monte Carlo.

decays of $\pi^0 \to \gamma\gamma$, some of this structure persists in angular distributions for $\bar{p}p \to \pi^0\pi^0$. It appears that the Monte Carlo correctly simulates this effect, since we find no corresponding structure in reconstructed angular distributions.

Figs. 8 to 13 show angular distributions from 1525 to 600 MeV/c in the same formats as Figs. 4 to 6.

The angular distributions of Figs. 4 to 6 and 8 to 13 have been fitted in terms of Legendre polynomials:

$$\frac{d\sigma}{d\Omega} = \sum_{\ell=0}^{\ell_{max}} a_\ell P_\ell^0(\cos\theta).$$

Results are given in Table 2. Terms up to $\ell = 6$ are required at 600 MeV/c, up to $\ell = 8$ from 900 to 1642 MeV/c, and up to $\ell = 10$ at 1800 and 1942 MeV/c.

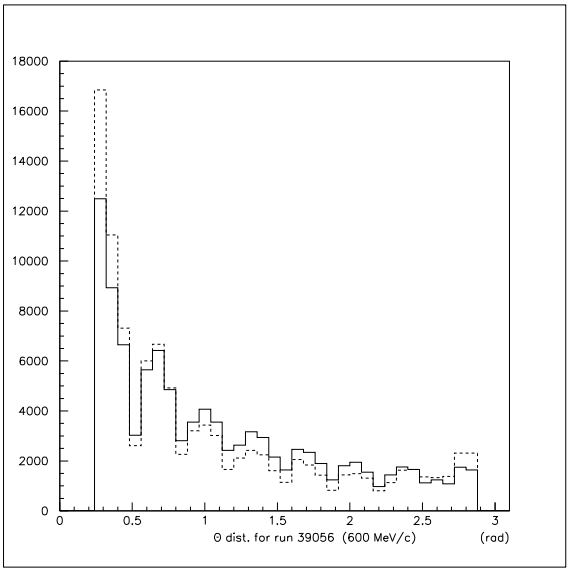

Fig. 7. Angular distribution of PEDs; the full histogram is for events in the full energy peak and the dashed curve is irrelevant for present purposes.

We do not show errors in the Table, since parameters are strongly correlated, and one would need the whole error matrix to be meaningful. The correlation arises because of the lack of acceptance above $\cos\theta = 0.85$. It is better to fit data directly than go through the intermediate step of Legendre coefficients.

5 Amplitude Analysis

Formulae for differential cross sections in terms of partial wave amplitudes are taken from the paper of Hasan and Bugg [1]. The differential cross section may be expressed in terms of spin-flip (F_{+-}) and non-flip (F_{++}) helicity amplitudes:

$$d\sigma/d\Omega = |F_{++}|^2 + |F_{+-}|^2 \tag{1}$$

$$F_{++} = \frac{1}{4}\sum_{J=0}^{J_{max}} (2J+1) f^J_{++} P_J(\cos\theta) \tag{2}$$

$$F_{+-} = \frac{1}{4}\sum_{J=1}^{J_{max}} \frac{(2J+1)}{\sqrt{J(J+1)}} f^J_{+-} P^1_J(\cos\theta). \tag{3}$$

Here P^m_J are Legendre polynomials.

The partial helicity amplitude f^J are defined in terms of angular momentum partial waves $T_{L,J}$ according to:

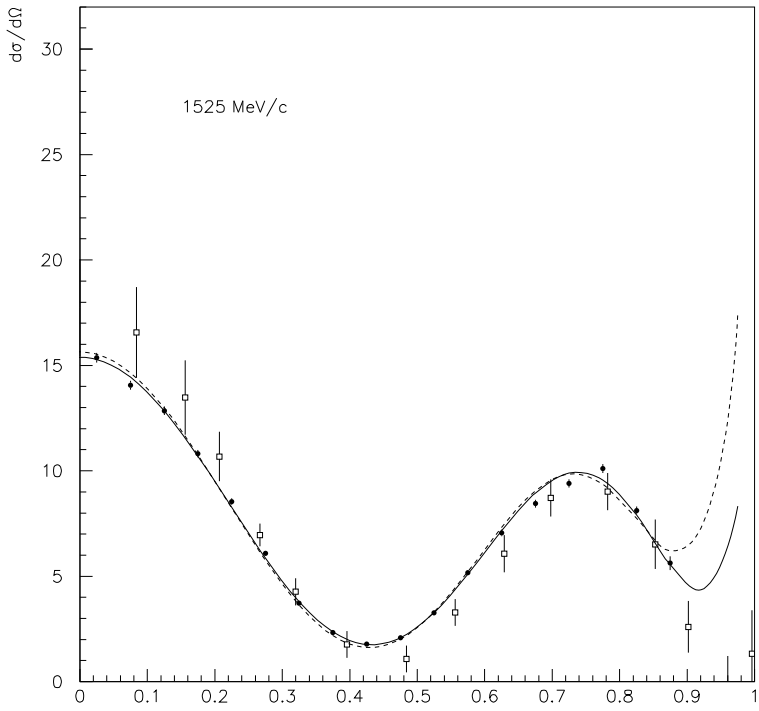

Fig. 8. As Fig. 4 at 1525 MeV/c.

$$\sqrt{2J+1}f^J_{++} = \sqrt{J}T_{J-1,J} - \sqrt{J+1}T_{J+1,J} \tag{4}$$

$$\sqrt{2J+1}f^J_{+-} = \sqrt{J+1}T_{J-1,J} - \sqrt{J}T_{J+1,J}. \tag{5}$$

We express the $T_{L,J}$ as sums over resonances, up to 3 for each J value:

$$T_{L,J} = \sum_{i=1}^{3} \frac{G_i B_L(p) B_J(q)}{s - M_i^2 - i M_i \Gamma_i}, \tag{6}$$

where B_L are standard Blatt-Weisskopf centrifugal barrier factors for angular momentum L in terms of momentum p in the entrance channel $\bar{p}p$ and q in the exit $\pi^0\pi^0$ channel. The radius of interaction is adjusted to 0.92 fm to obtain the $f_4(2050)$ peak at the right place, using PDG values of mass and width for that resonance: $M = 2044$ MeV, $\Gamma = 208$ MeV. The G_i are complex coupling constants.

The 0^+ amplitude has been alternatively fitted to a polynomial in s.

One fit to all momenta takes approximately 15 seconds of computing. There-

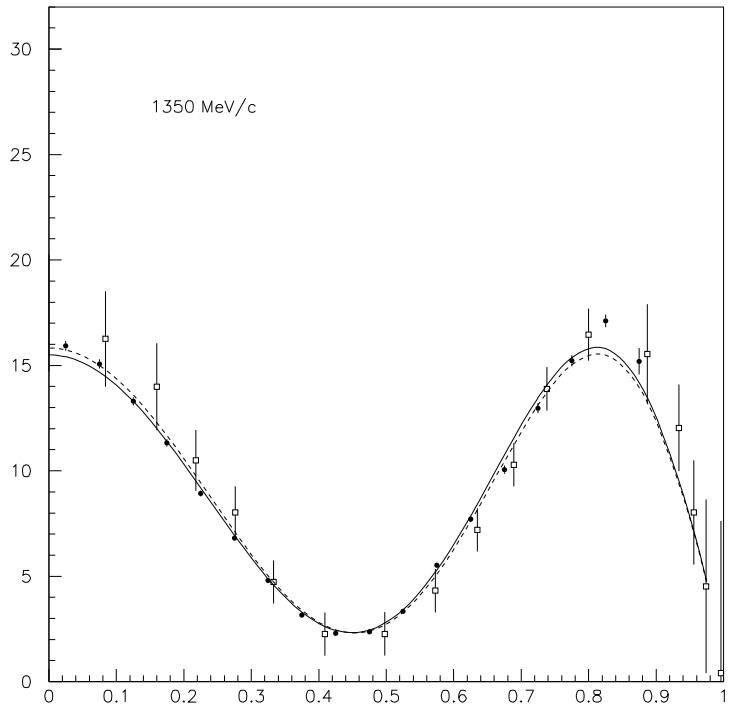

Fig. 9. As Fig. 4 at 1350 MeV/c. The open squares show a comparison with data of Dulude et al at 1361 MeV/c.

fore we have been able to investigate a large variety of solutions. We have found two stable solutions giving good fits to data at all momenta. The reason for the existence of this ambiguity is not difficult to find. The angular distribution for successive partial waves in terms of $z = \cos\theta$ are as follows:

$$^3P_0 = 1 \tag{7}$$
$$^3P_2 = 1 + 3z^2 \tag{8}$$
$$^3F_2 = 1 - 2z^2 + 5z^4 \tag{9}$$
$$^3F_4 = 3 + 15z^2 - 55z^4 \tag{10}$$
$$^3H_4 = O(z^8). \tag{11}$$

If only waves up to $^3F_2$ were present, the solution would be unique. However, the $^3F_4$ cross section may be expressed as a linear combination of $^3F_2$, $^3P_2$ and $^3P_0$. Then $^3H_4$ adds amplitudes up to powers of z^8; it is required at 900 MeV/c and above. Interferences between partial waves help to some extent, but do not eliminate the basic ambiguity. At the highest two momenta, a small contribution from $^3H_6$ is required, but only its interference with other waves

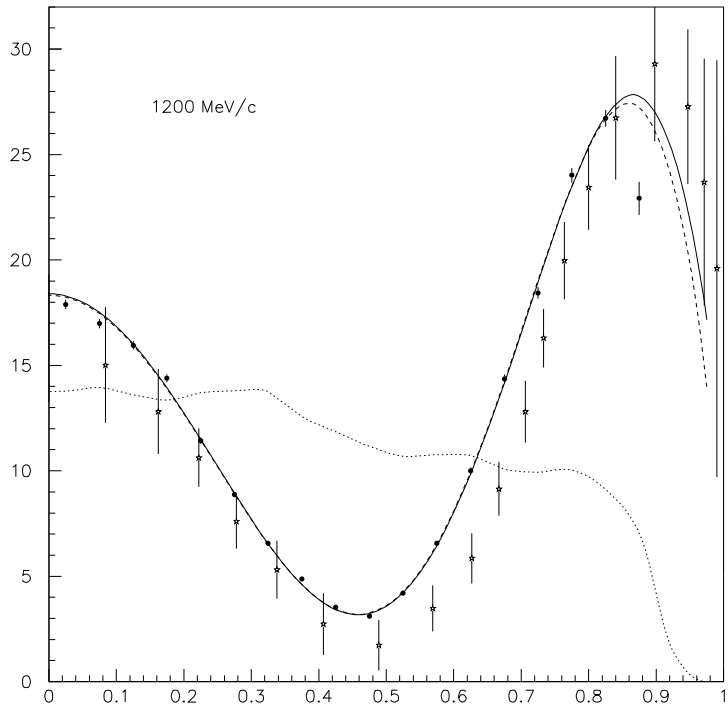

Fig. 10. As Fig. 6 at 1200 MeV/c. The dotted line show the acceptance derived from the Monte Carlo. No fit is able to accomodate the last point at $\cos\theta = 0.85$, so we reject it.

is significant and generates terms up to z^{10}. It is fitted with a Breit-Wigner resonance of mass 2540 MeV, $\Gamma = 250$ MeV, but these parameters are not at all critical. If it is omitted, χ^2 doubles.

In principle, there may be many further Barrelet ambiguities. Starting at the lowest momentum, there is a unique solution. When a dip of the differential cross section crosses $\cos\theta = 1$, a Barrelet ambiguity arises in principle. If one is lucky, the use of analytic functions eliminates this ambiguity, by relating real and imaginary parts of partial wave amplitudes as a function of s. We seem to be lucky. We have tried many tests starting the fit from random initial values. Also we have systematically swopped the sign of every resonance amplitude one by one and restarted the solution. We have also reversed signs of full partial wave amplitudes one by one. We find only two stable solutions.

The χ^2 of the two fits are 161 for solution 1 and 132 for solution 2; there are 161 differential cross sections and 9 normalisation parameters for the in-

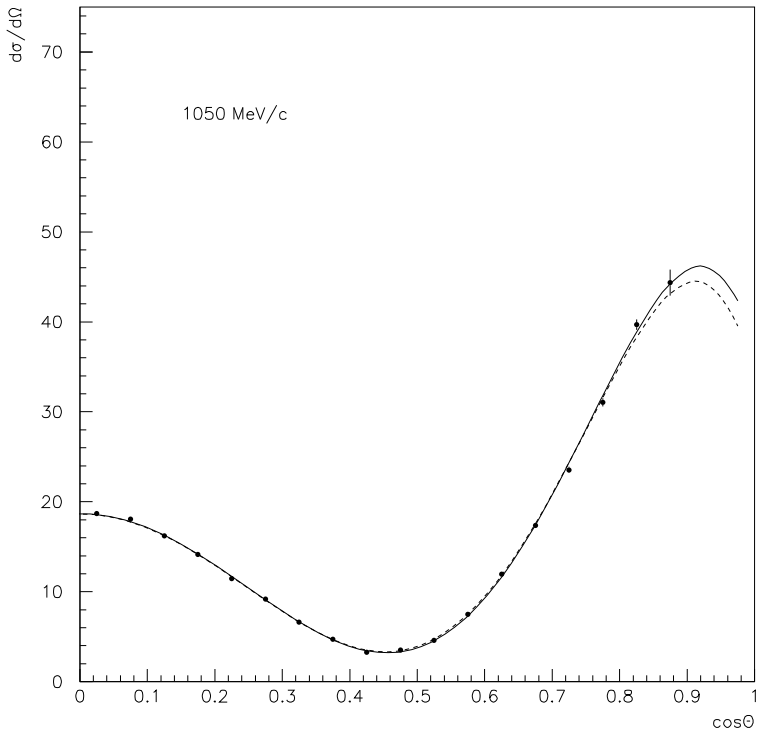

Fig. 11. As Fig. 4 at 1050 MeV/c.

tegrated cross section, fitted by 35 parameters for coupling constants, masses and widths. The spin 6 contribution is small and affects differential cross sections by amounts which are barely visible by eye.

Cross sections for individual partial waves from these two solutions are displayed in Fig. 14. Both solutions require some 4^+ contribution around 2050 MeV. The peak of the resonance is moved to about 2090 MeV by the effect of the centrifugal barrier in the $\bar{p}p$ channel. A further 4^+ resonance is required around 2300 MeV in both solutions.

For 2^+, both solutions require a resonance close to 2010 MeV. There is some further activity in the high mass region, but one cannot deduce precisely what contributes there. In $\pi\pi$, a phase advance is observed suggesting a further resonance around 2300 MeV. The $\eta\eta$ data, reported separately, require a resonance at 2300 ± 20 MeV, and this has been used to fit the $\pi\pi$ data, though its parameters are not critical there.

For 0^+, a fairly smoothly dropping amplitude is required in solution 1. Some-

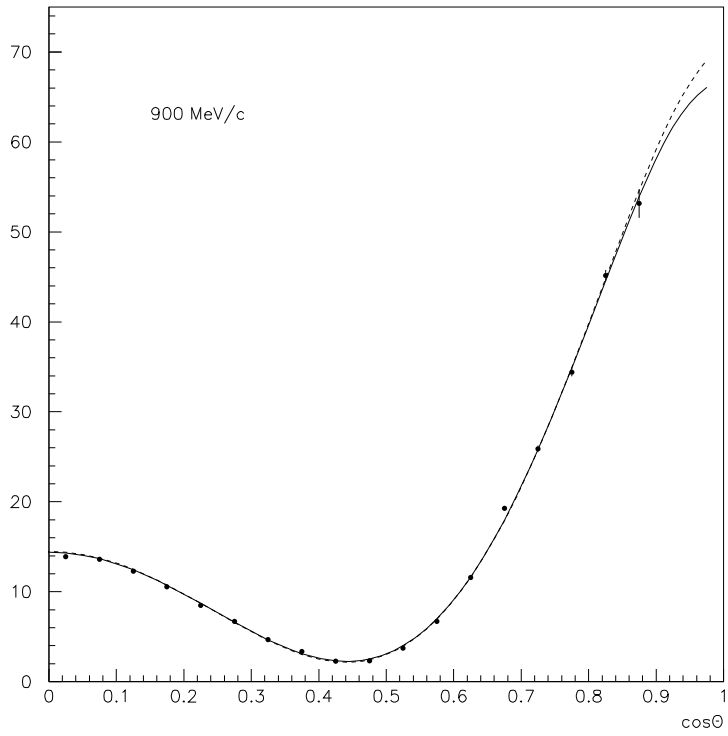

Fig. 12. As Fig. 4 at 900 MeV/c.

thing is required around 2100 MeV and could be identified with the $f_0(2100)$ which has been confirmed in Crystal Barrel data on $\bar{p}p \to \eta\eta\pi^0$. The data on $\bar{p}p \to \eta\eta$ show a strong requirement for $f_0(2100)$, which is therefore included in the fit to $\pi\pi$, but it makes only a small contribution there. In solution 2, there are peaks around 2000 and 2320 MeV. The former may be a threshold effect and has been fitted with a resonance below threshold. The latter might be a further 0^+ resonance, but the fits are indecisive about this.

Table 3 list the masses and widths of those resonances definitely required by $\pi^0\pi^0$ data alone. Errors on masses and widths cover three standard deviation increases in χ^2 when each parameter is scanned and all remaining parameters are re-optimised, including masses and widths of other resonances. Correlations between parameters of f_2 and f_4 resonances are small. In solution 2, relative amounts of ${}^3F_4$ and ${}^3H_4$ are close to those fitted to data on $\bar{p}p \to \pi^-\pi^+$ by Hasan and Bugg, see their Fig. 3. It is also very close to that found by Bing Song Zou for $\eta\pi^0\pi^0$ data. For those reasons, we anticipate that solution 2 is more likely to be the correct one.

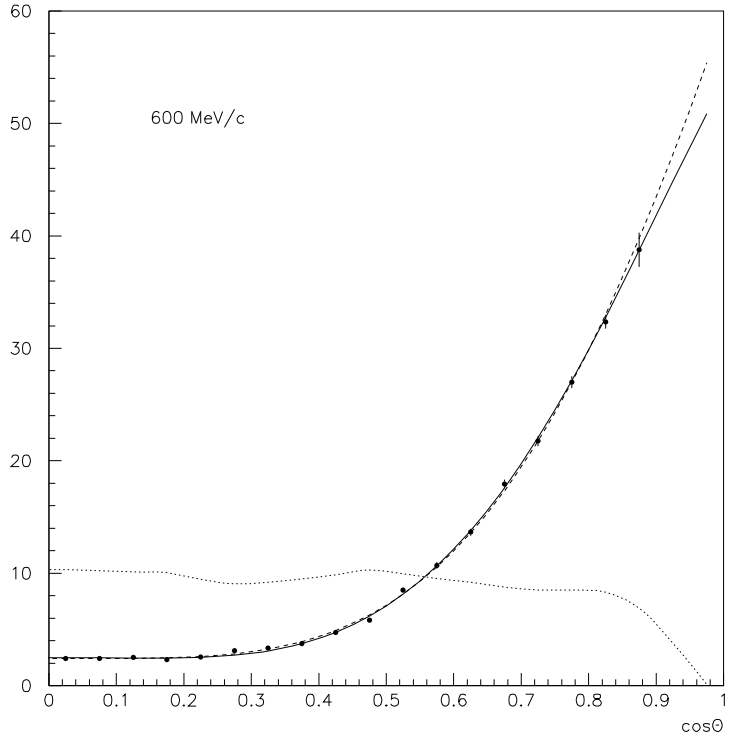

Fig. 13. As Fig. 6 at 600 MeV/c.

There is extensive evidence elsewhere for $f_4(2300)$. It was required in all earlier partial wave analyses of $\bar{p}p \to \pi^-\pi^+$. It is also observed clearly in VES data on the $\eta\pi^+\pi^-$ final state [2], decaying to $f_2(1270)\eta$ with $M = 2330 \pm 10(stat.) \pm 20(syst)$ MeV, $\Gamma = 225 \pm 20 \pm 40$ MeV. It is also clearly visible in VES data on the $\omega\omega$ final state [3]. From an analysis of Crystal Barrel data on $\bar{p}p \to \eta\pi^0\pi^0$, Zou finds an $f_4(2320\pm30)$, with $\Gamma = 220\pm30$ MeV, decaying to both $a_2(1320)\pi$ and $f_2(1270)\eta$, mainly the latter. Hasan and Bugg found an f_4 with mass 2314 MeV and $\Gamma = 278$ MeV [1].

Zou also finds the requirement for $f_2(2020 \pm 40)$ with $\Gamma = 235 \pm 70$ MeV. Hasan and Bugg found an f_2 with $M = 1996$ MeV and a width of 134 MeV.

References

[1] A. Hasan and D.V. Bugg, Phys. Lett. B334 (1994) 215.

[2] D. Ryabchikov, Hadron'97 Proceedings, p. 603.

Momentum (Mev/c)	χ^2	a_0	a_2	a_4	a_6	a_8	a_{10}
600	25.0	57.2	135.9	50.9			
	10.7	53.8	121.5	33.3	-10.5		
900	40.0	113.7	234.2	153.5	-73.2		
	17.7	102.8	188.1	91.5	-120.5	-21.2	
1050	11.8	120.1	173.7	118.8	-122.1	5.3	
1200	9.1	92.0	41.5	8.7	-184.0	-7.7	
1350	14.6	78.7	30.0	41.2	-117.1	40.3	
1525	13.8	64.4	-25.9	26.4	-94.6	84.4	
1642	11.7	60.3	-9.1	64.3	-25.3	128.8	
1800	52.2	54.4	40.1	103.7	66.2	148.5	
	24.1	47.0	5.1	57.6	17.8	111.8	-22.2
1940	15.8	46.4	29.4	71.2	55.0	97.9	-25.0

Table 2
Coefficients of the Legendre series fitted to angular distributions.

J^P	M (MeV/c^2)	Γ (MeV/c^2)	M (MeV/c^2)	Γ (MeV/c^2)
4^+	2044	208	2044	208
4^+	2295 ± 15	230 ± 20	2290 ± 10	230 ± 25
2^+	2010 ± 20	180 ± 35	2015 ± 20	180 ± 30

Table 3
Masses and widths of fitted 4^+ and 2^+ resonances; columns 2 and 3 show solution 1 and columns 4 and 5 solution 2.

[3] D. Ryabchikov, private communication.

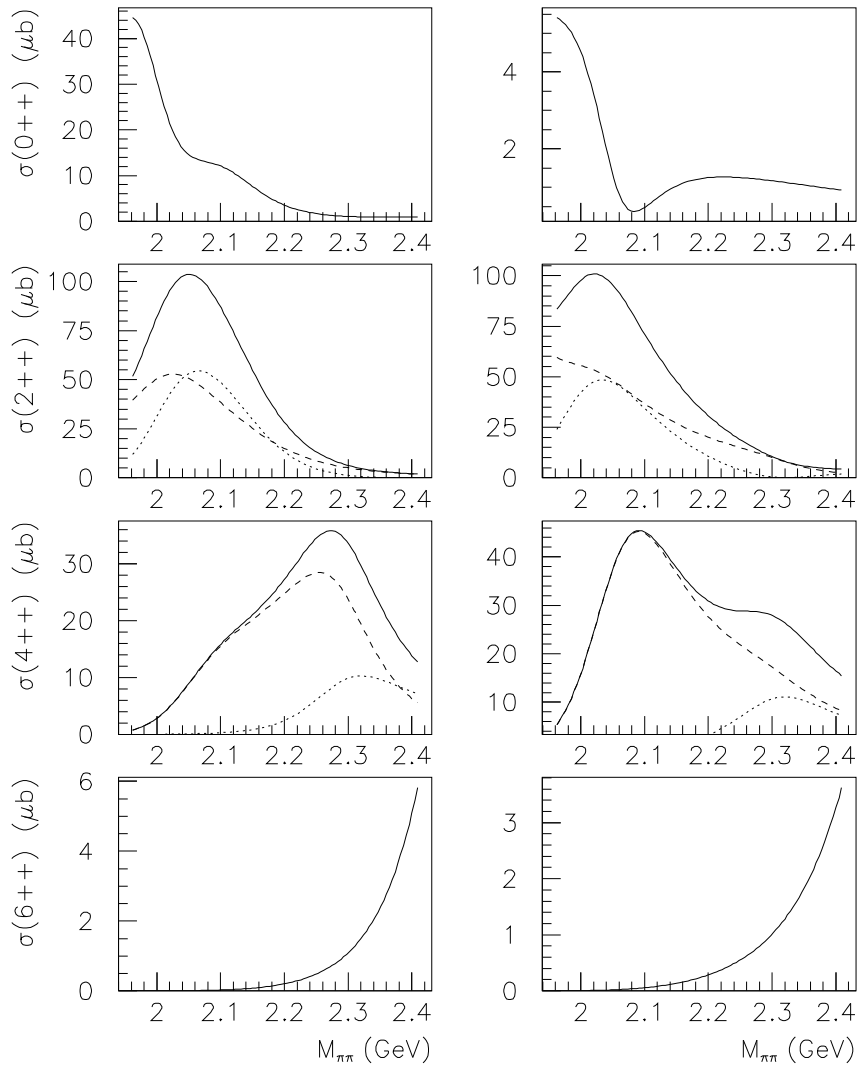

Fig. 14. Intensities fitted to 0^+, 2^+, 4^+ and 6^+ v. $\pi\pi$ mass. The left-hand column shows solution 1 and the right-hand column the preferred solution 2. Dashed curves show $^3P_2$ and $^3F_4$ cross sections and dotted curved $^3F_2$ and $^3H_4$ intensities; their sum is shown by the full curves